

Research Article

Surface Structure and Catalytic Performance of Ni-Fe Catalyst for Low-Temperature CO Hydrogenation

Fanhui Meng, Pengzhan Zhong, Zhong Li, Xiaoxi Cui, and Huayan Zheng

Key Laboratory of Coal Science and Technology, Ministry of Education and Shanxi Province, Taiyuan University of Technology, Taiyuan, Shanxi 030024, China

Correspondence should be addressed to Zhong Li; lizhong@tyut.edu.cn

Received 6 December 2013; Revised 19 February 2014; Accepted 21 February 2014; Published 24 March 2014

Academic Editor: Anton Kokalj

Copyright © 2014 Fanhui Meng et al. This is an open access article distributed under the Creative Commons Attribution License, which permits unrestricted use, distribution, and reproduction in any medium, provided the original work is properly cited.

Catalysts $16\text{Ni}_x\text{Fe}/\text{Al}_2\text{O}_3$ (x is 0, 1, 2, 4, 6, 8) were prepared by incipient wetness impregnation method and the catalytic performance for the production of synthetic natural gas (SNG) from CO hydrogenation in slurry-bed reactor were studied. The catalysts were characterized by BET, XRD, UV-Vis DRS, H_2 -TPR, CO-TPD, and XPS, and the results showed that the introduction of iron improved the dispersion of Ni species, weakened the interaction between Ni species and support and decreased the reduction temperature and that catalyst formed Ni-Fe alloy when the content of iron exceeded 2%. Experimental results revealed that the addition of iron to the catalyst can effectively improve the catalytic performance of low-temperature CO methanation. Catalyst $16\text{Ni}_4\text{Fe}/\text{Al}_2\text{O}_3$ with the iron content of 4% exhibited the best catalytic performance, the conversion of CO and the yield of CH_4 reached 97.2% and 84.9%, respectively, and the high catalytic performance of Ni-Fe catalyst was related to the property of formed Ni-Fe alloy. Further increase of iron content led to enhancing the water gas shift reaction.

1. Introduction

The production of synthetic natural gas (SNG) from coal or biomass has attracted much attention in recent years, especially in China, because of the increasing demands for natural gas and the wish for enhancing domestic energy security [1, 2]. The gasification of coal results in the production of syngas containing mainly H_2 and CO; after the gas cleaning, the H_2/CO ratio of the syngas can be adjusted to suitable ratio by water-gas shift reaction (WGS) and finally the syngas can be converted to SNG through CO methanation. Among the SNG production processes, the methanation of syngas is one of the most critical steps, and the methanation reaction is a strong exothermic reaction; for every 1% of CO completely converted into CH_4 , gas adiabatic temperature rise is approximately 70°C [3]. Thus, the major challenge is to remove in time the highly exothermic heat effectively. Recently, many efforts have been made to develop a number of methanation reactors for SNG production, including fixed-bed [1, 4], fluidized-bed [5–7], and slurry-bed reactors [8, 9]. Among them, the slurry-bed reactor can remove the reaction heat efficiently and keep the reaction

at isotherm low temperature so as to minimize the catalyst deactivation and avoid the limitation on CH_4 yield resulting from thermodynamic equilibrium [9, 10]. But to develop an active and stable low-temperature methanation catalyst for a slurry-bed reactor is more difficult, and now, only a few studies have been done in the laboratory [11, 12].

Numerous catalysts have been used for fixed-bed methanation reaction [9]. Among these catalysts, Ni-based catalysts have been widely employed due to the relatively low cost, high activity, and high selectivity to methane [13–16]. It is known that conventional Ni-based catalysts showed high catalytic activity at the high reaction temperature; however, the catalytic activity of CO conversion and CH_4 selectivity was low at the low reaction temperature. To overcome this problem, addition of second metal such as Sm, Ce, and Fe has been attempted to enhance the catalytic activity and stability of Ni-based catalysts for CO methanation reaction, because the second metal can improve the dispersion of active metal and adjust the interaction between Ni and the support [17–20]. Hwang et al. [18, 19] prepared nickel-M-Al xerogel (NiMAX) catalysts doped with different second metal ($M = \text{Fe}, \text{Ni}, \text{Co}, \text{Ce},$ and La) by sol-gel method, and they found

that NiFeAX catalyst exhibited the best catalytic performance for CO or CO₂ methanation at low reaction temperature (220°C and 230°C). Therefore, the investigations over the Ni-Fe catalysts for the low-temperature CO methanation in slurry-bed would be worthwhile.

Our previous work [21, 22] has optimized the nickel precursor and Al₂O₃ support of Ni-Fe/Al₂O₃ catalysts for CO methanation. In this work, a series of Ni-Fe/Al₂O₃ catalysts with different Fe content were prepared by incipient wetness impregnation method and characterized by BET, XRD, UV-Vis DRS, H₂-TPR, CO-TPD, and XPS. The effects of Fe content on surface structure and catalytic performance of the catalysts for low-temperature CO methanation in slurry-bed reactor were studied.

2. Experiment

2.1. Catalyst Preparation. The commercial γ -Al₂O₃ (100–140 mesh, supported by Shandong Alumina Company) precalcined at 550°C for 6 h was used in this study. The Ni-based catalysts were prepared by incipient wetness impregnation method, described as follows: nickel nitrate hexahydrate (Sinopharm Chemical Reagent Co., Ltd) and ferric nitrate nonahydrate (Sinopharm Chemical Reagent Co., Ltd) were dissolved in deionized water, followed by the addition of γ -Al₂O₃: the slurry was continuously stirred at room temperature for 24 h and then dried at 120°C for 12 h and calcined at 450°C for 4 h in muffle oven; and the obtained sample was reduced at 550°C for 6 h in a flow of 25% H₂ diluted with nitrogen. The above catalysts were denoted as 16Ni_xFe/Al₂O₃, where 16 represents the weight percent of Ni, x represents the weight percent of Fe, and x is 0, 1, 2, 4, 6, and 8. In addition, catalyst 8Fe/Al₂O₃ and commercial catalyst named J108-2Q (supported by Sichuan Shutai chemical technology Co., Ltd) were used as reference counterparts.

2.2. Characterization. X-Ray diffraction (XRD) data were obtained with Rigaku D/max 2500 diffractometer (Cu K α radiation, $\lambda = 0.154056$ nm) at 40 kV and 100 mA, and the crystallite sizes were estimated from XRD patterns applying the Scherrer equation.

The BET specific surface area, pore volume, and the average pore diameter of samples were measured by the multipoint BET analysis method using N₂ adsorption isotherms at 77 K. The measurement was performed on Micrometrics ASAP 2100 automatic device.

X-ray photoelectron spectroscopy (XPS) data were collected on Thermo Fisher ESCALAB 250Xi with Al K α radiation. The binding energies were calibrated by the carbon (C1s = 284.8 eV).

Ultraviolet-visible diffuse reflectance spectra (UV-VIS DRS) were performed at room temperature in the range of 250–800 nm by a CARY 300 spectrophotometer, using MgO as the reference material.

Temperature-programmed reduction of H₂ (H₂-TPR) and temperature-programmed desorption of CO (CO-TPD) experiments were carried out with Micrometrics Autochem II 2920 model multifunctional adsorption instrument. Prior

to the TPR measurements, 20 mg of the samples was pre-treated at 350°C for 0.5 h in flowing He (50 mL/min), after cooling the reactor to room temperature, a 10% H₂/90% Ar (50 mL/min) gas mixture was introduced, and the sample was heated to 800°C. Prior to the TPD measurements, 40 mg of the samples was reduced at 550°C and then cooled to 50°C. 10% CO diluted in He was passed through the sample until saturation, and the TPD profile was obtained by heating the sample from 50°C to 800°C.

2.3. Catalytic Activity Evaluation. Catalytic performance evaluation was carried out in a 250 mL slurry-bed agitated autoclave. In each experiment, 2.0 g of catalyst (100–140 mesh particle) and 120 mL of paraffin (boiling point higher than 350°C) were added into the reactor vessel and rotated at 750 r/min. N₂ (99.995%) was introduced into the reactor at a flow rate of 50 mL/min to remove the air and the reactor was heated at a rate of 2°C/min from room temperature to 280°C. Then, the syngas of H₂ (99.995%) and CO (99.9%) was switched as feed gas at 75 mL/min and 25 mL/min, respectively, to synthesize methane at 1.0 MPa with the space velocity of 3000 mL/g_{cat} · h. The products from the reactor were condensed by ethanol at 2°C, the cooling liquid was removed by gas-liquid separator, and the outlet gas was quantitatively analyzed by on-line gas chromatography (Agilent 7890A), which was equipped with flame ionization detector (FID) and thermal conductivity detector (TCD), using He as carrier gas. FID detector equipped with HP-AL/S column (30 m × 530 μ m × 15 μ m) was used to analyze C_{1–4}, and TCD detector equipped with Porapak-Q column (6 ft × 1/8 inch), HP-PLOT/Q column (30 m × 530 μ m × 40 μ m), and HP-MOLESIEVE column (30 m × 530 μ m × 25 μ m) was used to analyze CO, N₂, and CO₂. The temperature of FID and TCD was 300°C and 250°C, respectively.

The conversion of CO, the selectivity of CH₄, CO₂, and C_{2–4}, and the yield of CH₄ were calculated using the following expressions:

$$\begin{aligned}
 X_{\text{CO}} &= \frac{F(\text{CO}_{\text{in}}) - F(\text{CO}_{\text{out}})}{F(\text{CO}_{\text{in}})} \times 100\%, \\
 S_{\text{CH}_4} &= \frac{F(\text{CH}_{4,\text{out}})}{F(\text{CO}_{\text{in}}) - F(\text{CO}_{\text{out}})} \times 100\%, \\
 S_{\text{CO}_2} &= \frac{F(\text{CO}_{2,\text{out}})}{F(\text{CO}_{\text{in}}) - F(\text{CO}_{\text{out}})} \times 100\%, \\
 S_{\text{C}_i} &= \frac{i \times F(\text{C}_{i,\text{out}})}{F(\text{CO}_{\text{in}}) - F(\text{CO}_{\text{out}})} \times 100\% \quad (i = 2, 3, 4), \\
 Y_{\text{CH}_4} &= X_{\text{CO}} \times S_{\text{CH}_4},
 \end{aligned} \tag{1}$$

where X_{CO} , S_{CH_4} , S_{C_i} , S_{CO_2} , and Y_{CH_4} refer to the conversion of CO; the selectivity of CH₄, C_{2–4}, and CO₂; and the yield of CH₄, respectively. C_{2–4} represents C₂H₄, C₂H₆, C₃H₆, C₃H₈, C₄H₈, and C₄H₁₀. F and W_{cat} represent the flow of CO, C_{2–4}, CH₄, and CO₂ (mL/min, STP) and the weight of catalyst, respectively.

TABLE 1: Catalytic performance of 16Ni_xFe/Al₂O₃ catalysts for CO methanation in slurry-bed reactor.

Catalysts	X_{CO} (%)	Selectivity (%)			Y_{CH_4} (%)
		CH ₄	CO ₂	C ₂₋₄	
16Ni/Al ₂ O ₃	82.5	87.4	7.8	4.8	72.1
16Ni1Fe/Al ₂ O ₃	92.9	81.9	7.4	10.7	76.1
16Ni2Fe/Al ₂ O ₃	96.4	86.7	7.7	5.6	83.6
16Ni4Fe/Al ₂ O ₃	97.2	87.3	8.6	4.1	84.9
16Ni6Fe/Al ₂ O ₃	94.8	84.4	10.8	4.7	80.0
16Ni8Fe/Al ₂ O ₃	92.6	81.0	13.6	5.5	75.0
8Fe/Al ₂ O ₃	10.6	78.1	15.4	6.6	8.3
J108-2Q	88.9	82.7	3.4	13.9	73.5

3. Results and Discussion

3.1. Catalytic Performance of 16Ni_xFe/Al₂O₃ Catalysts for CO Methanation. The catalytic performance of 16Ni_xFe/Al₂O₃ catalysts with different iron content for low-temperature CO methanation in slurry-bed reactor is listed in Table 1. The reference catalyst 16Ni/Al₂O₃ showed the conversion of CO and the yield of CH₄ at 82.5% and 72.1%, respectively, which were much higher than that of catalyst 8Fe/Al₂O₃. However, the catalytic performance of the above two catalysts were lower than the commercial catalyst J108-2Q.

The introduction of iron in 16Ni_xFe/Al₂O₃ catalyst greatly improved the catalytic performance. A rise in iron content greatly enhanced CO conversion, reaching the maximum for the catalyst containing 4% iron content with outstanding conversion of CO and the yield of CH₄ at 97.2% and 84.9%, respectively. Further rise in iron content resulted in the decrease of catalytic performance. It is well known that Fe-based catalysts show high water gas shift activity, and it can be seen that the increase of iron content aggravated the water gas shifted reaction [23], resulting in the more production of CO₂. In addition, the selectivity of C₂₋₄ changed slightly with the increase of iron content except the catalyst with 1% iron content.

3.2. BET. Textural properties of γ -Al₂O₃ support and 16Ni_xFe/Al₂O₃ ($x = 0, 1, 4, 8$) catalysts are summarized in Table 2. The γ -Al₂O₃ support got a high BET surface area of 191 m²/g, and the pore volume and the average pore diameter were 0.38 cm³/g and 5.81 nm, respectively. After the loading of 16% Ni, part of nickel species began to aggregate and formed crystalline nickel oxide clusters, which may block the pores of γ -Al₂O₃ and thus make the BET surface area of catalyst 16Ni/Al₂O₃ decreases to 148 m²/g [4, 24]; in addition, both the pore volume and average pore diameter of catalyst 16Ni/Al₂O₃ decreased. However, the catalysts 16Ni_xFe/Al₂O₃ ($x = 1, 4, 8$) modified with iron showed a slightly higher BET surface area compared with 16Ni/Al₂O₃ catalyst, implying that the addition of iron improved the dispersion of Ni species and decreased the agglomeration; similar results were also reported in other literatures [4, 24, 25].

3.3. XRD. Figure 1(a) shows the XRD patterns of calcined catalysts 16Ni_xFe/Al₂O₃. The diffraction peaks of γ -Al₂O₃

TABLE 2: Textural properties of γ -Al₂O₃ support and 16Ni_xFe/Al₂O₃ catalysts.

Sample	BET surface area (m ² /g)	Pore volume (cm ³ /g)	Average pore diameter (nm)
γ -Al ₂ O ₃	192	0.38	5.81
16Ni/Al ₂ O ₃	148	0.28	5.50
16Ni1Fe/Al ₂ O ₃	153	0.28	5.42
16Ni4Fe/Al ₂ O ₃	158	0.27	5.31
16Ni8Fe/Al ₂ O ₃	151	0.27	5.24

were presented at 2θ angle of 37.4°, 45.8°, and 66.9°, and characteristic diffraction peaks due to NiO were observed at 2θ of 37.4°, 43.6°, and 63.1°, and no diffraction peaks of nickel nitrate hexahydrate were observed, indicating that Ni species in 16Ni_xFe/Al₂O₃ catalyst were mainly presented as NiO. It is interesting to note that the characteristic peaks of NiO gradually decreased with the increase of iron content. In addition, no diffraction peaks of iron species were observed in XRD patterns even if the content of iron reached 8%.

Figure 1(b) displays the XRD patterns of reduced catalysts 16Ni_xFe/Al₂O₃. It can be seen that all the reduced catalysts exhibited the characteristic peaks of Ni at 2θ angle of 44.3°, 51.8° and 76.0°, indicating that NiO was reduced to metallic Ni. The diffraction peaks due to iron species were not detected. It is noted that, compared with reference catalyst 16Ni/Al₂O₃, the diffraction peak of catalysts 16Ni_xFe/Al₂O₃ ($x \geq 2$) exhibited lower angles by increasing the iron content; although this change was not obvious, it is an effect of a significant interaction between iron and Ni, and the reason was due to the formation of Ni-Fe alloy, which appeared at 44.3°, 51.5°, and 75.9° [20, 26], and the intensity of metal Ni decreased, indicating that the crystallite size of Ni decreased. Combined with the catalytic performance listed in Table 1, the results suggested that the formation of Ni-Fe alloy must be an important factor for CO methanation reaction over the Ni species that existed in the catalysts.

3.4. UV-Vis DRS. Figure 2 depicts the UV-Vis DRS of calcined 16Ni_xFe/Al₂O₃ catalysts. The absorption band position was determined by the first-derivative of absorption bands [27]. It can be seen that all catalysts showed the absorption bands (optical absorption threshold) in the range of 300~

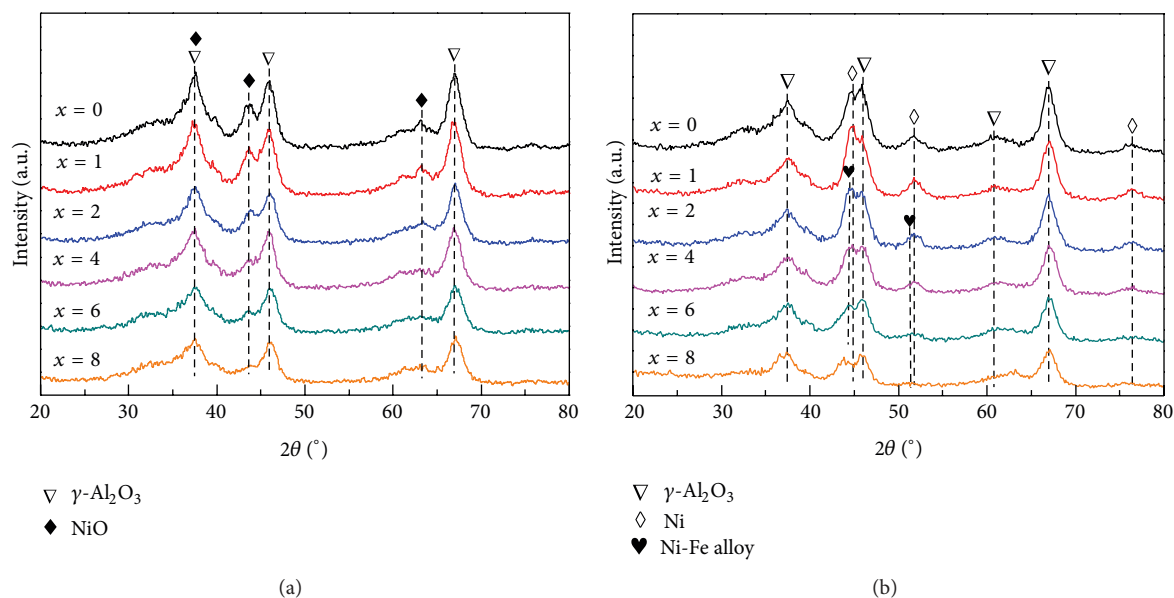


FIGURE 1: XRD patterns of catalysts $16\text{Ni}_x\text{Fe}/\text{Al}_2\text{O}_3$: (a) calcined and (b) reduced.

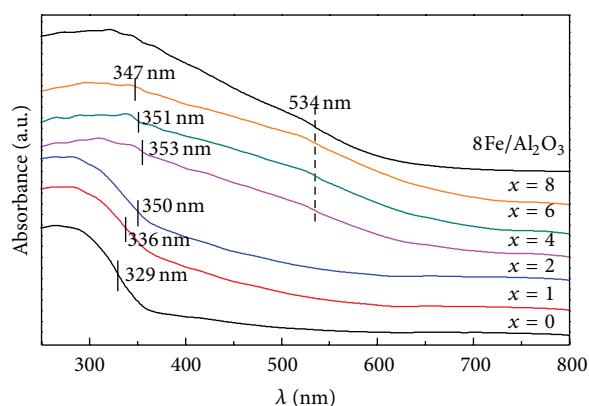


FIGURE 2: UV-Vis DRS of calcined catalysts $16\text{Ni}_x\text{Fe}/\text{Al}_2\text{O}_3$.

600 nm. Compared with catalyst $16\text{Ni}/\text{Al}_2\text{O}_3$ (329 nm), the absorption bands of $16\text{Ni}_x\text{Fe}/\text{Al}_2\text{O}_3$ catalysts in the spectra were all red-shifted with the increase of iron content, and the maximum absorption band at 353 nm was found on catalyst $16\text{Ni}_4\text{Fe}/\text{Al}_2\text{O}_3$, indicating that there was a strongly interaction between Ni species and iron species [28]. While for the catalyst $8\text{Fe}/\text{Al}_2\text{O}_3$, the absorption band was exhibited at 534 nm, which can be ascribed to the existence of Fe_2O_3 species [29]. Catalysts $16\text{Ni}_x\text{Fe}/\text{Al}_2\text{O}_3$ with the iron content above 4% also exhibited the same absorption band position at 534 nm, except for the absorption band in the range of 300~400 nm. The results indicated that part of iron existed as Fe_2O_3 , although it was not detected by XRD patterns in Figure 1(a).

3.5. H_2 -TPR. The H_2 -TPR profiles of $16\text{Ni}_x\text{Fe}/\text{Al}_2\text{O}_3$ catalysts are shown in Figure 3. For comparison, the TPR profile of catalyst $8\text{Fe}/\text{Al}_2\text{O}_3$ is also presented in Figure 3. The

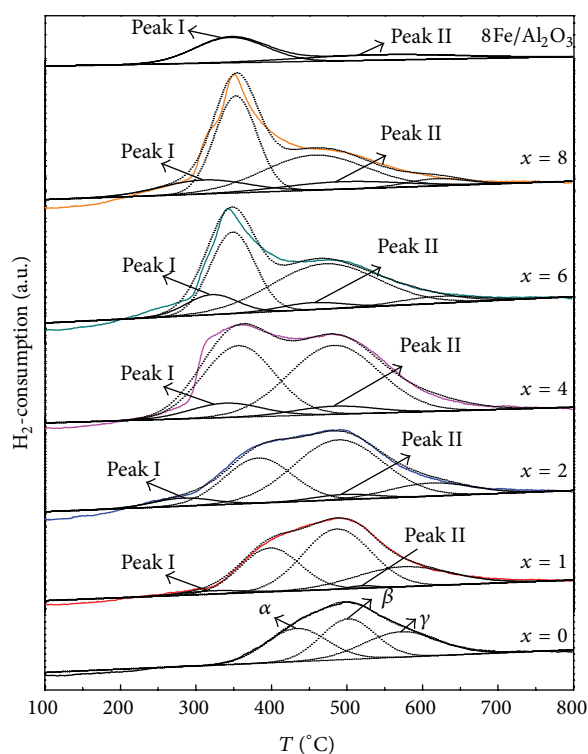


FIGURE 3: H_2 -TPR profiles of catalysts $16\text{Ni}_x\text{Fe}/\text{Al}_2\text{O}_3$.

reducible NiO species over the Al_2O_3 support are classified into three types: α , β , and γ [15, 30]. The overlapped peaks in the temperature range of 200~440°C were ascribed to the reduction peak of $\text{Fe}_2\text{O}_3 \rightarrow \text{Fe}_3\text{O}_4$ (peak I) and the reduction of α -NiO, which weakly interacted with or kept away from Al_2O_3 support; the peaks in the range of 440~600°C were assigned to the reduction peak of $\text{Fe}_3\text{O}_4 \rightarrow \text{Fe}$

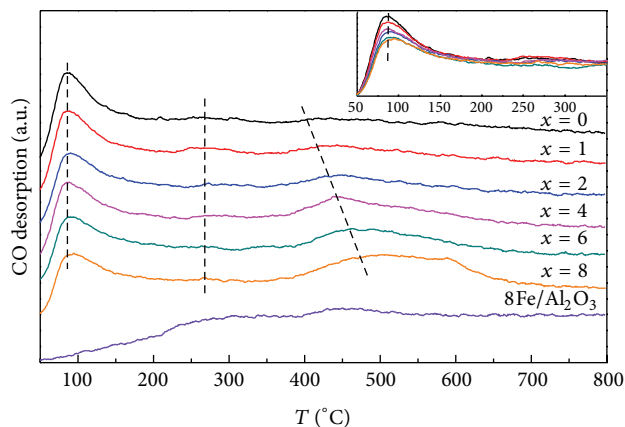


FIGURE 4: CO-TPD profiles of the reduced catalysts $16\text{Ni}_x\text{Fe}/\text{Al}_2\text{O}_3$.

(peak II) and the reduction peak of β -NiO, which had a strong interaction state with the support; additionally, the reduction peak in the range of $550\sim 750^\circ\text{C}$ was mainly attributed to the reduction of NiAl_2O_4 spinel [31, 32].

After the introduction of iron, the reduction peaks of $16\text{Ni}_x\text{Fe}/\text{Al}_2\text{O}_3$ shifted to lower temperature, and the total reduction peak areas increased gradually with the increase of iron content, indicating that the addition of iron facilitated the reduction of catalysts. It is believed that the addition of iron weakened the interaction between Ni and Al_2O_3 support, changed the microchemical environment of Ni and iron species on the surface of the catalyst, and thus increased the amount of reduction species [33–35].

In order to clarify the effect of iron content on the reduction of Ni species, Gaussian fitting analysis was conducted, and the reduction peak area of Ni species was obtained by subtracting the reduction peak area of corresponding Fe content from the total hydrogen consumption of each catalyst; the results are shown in Figure 3 and Table 3. According to the iron content of $16\text{Ni}_x\text{Fe}/\text{Al}_2\text{O}_3$ catalysts and taking the hydrogen consumption of $8\text{Fe}/\text{Al}_2\text{O}_3$ catalyst as a benchmark, it can be seen that the total hydrogen consumption increased with the increase of iron content, which was due to the reduction of Fe species and the Ni species. Catalyst $16\text{Ni}/\text{Al}_2\text{O}_3$ got the smallest amount of α reduction peak, and the amount of α peak increased gradually with the increase of iron content, while the amount of γ reduction peak decreased, indicating that the increase of iron content improved the reduction species of NiO. Among the catalysts examined, when the iron content reached 4%, the amount of β reduction peak reached the maximum (45.3%); further increase of iron content resulted in the decrease of β peak amount. The results were consistent with the catalytic performance of catalysts $16\text{Ni}_x\text{Fe}/\text{Al}_2\text{O}_3$; thus, it can be concluded that the β -NiO species was the main reason for enhancing the catalytic activities of CO methanation. Similar results have been reported in Hu et al.'s study [15]. In addition, it can be seen that the reduction peak area of peak I of catalyst $8\text{Fe}/\text{Al}_2\text{O}_3$ was larger than peak II, and the shape of peak I was sharp, while peak II was broad, indicating that the reduction degree of Fe_2O_3 to Fe_3O_4 was high and the reduction rate was fast, while the reduction

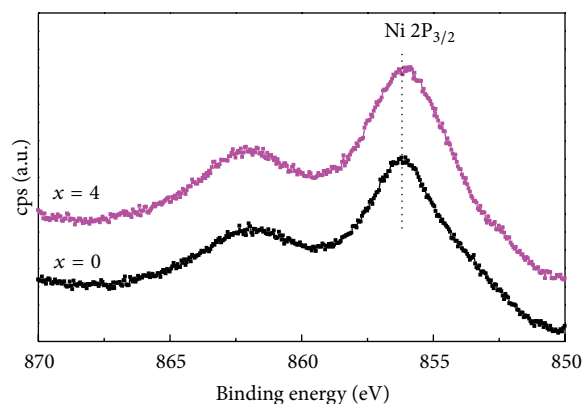


FIGURE 5: XPS spectra of the reduced catalysts $16\text{Ni}_x\text{Fe}/\text{Al}_2\text{O}_3$.

degree of Fe_3O_4 to Fe was low and the reduction rate was slow. With the increase of Fe content, the relative reduction content of Fe_2O_3 to Fe_3O_4 increased from 2.3% to 11.9%.

It is reported that Fe_3O_4 species was the main active component of water gas shift reaction [23], indicating that the catalyst with larger content of Fe_3O_4 favored more CO_2 production, and the results were in agreement with the catalytic performance listed in Table 1.

3.6. CO-TPD. Figure 4 shows the CO-TPD profiles of $16\text{Ni}_x\text{Fe}/\text{Al}_2\text{O}_3$ catalysts. All the catalysts exhibited a low-temperature peak centered at $\sim 85^\circ\text{C}$, which was attributed to the desorption of weak chemisorption or physical adsorption of CO. The weak peaks centered at around 265°C could be due to desorption of the middle intensive CO adsorption, and the highest desorption temperature shoulder spanning from 400 to $\sim 500^\circ\text{C}$ was probably attributed to the strong adsorption of CO [36]. It also can be seen that catalyst $8\text{Fe}/\text{Al}_2\text{O}_3$ exhibited almost no desorption peaks, which means that the adsorption of CO of catalysts $16\text{Ni}_x\text{Fe}/\text{Al}_2\text{O}_3$ was mostly attributed to the active component Ni and that the increase of CO adsorption amount was attributed to the increase of Fe content and the interaction between Fe and Ni. The former results of XRD, BET, and H_2 -TPR showed that the introduction of Fe improved the dispersion of Ni and increased the BET specific surface area and the amount of active component Ni which facilitated the adsorption of more CO.

3.7. XPS. Figure 5 shows the $\text{Ni } 2p_{3/2}$ core level spectra of reduced catalysts $16\text{Ni}/\text{Al}_2\text{O}_3$ and $16\text{Ni}_4\text{Fe}/\text{Al}_2\text{O}_3$. The binding energies of $\text{Ni } 2p_{3/2}$ for $16\text{Ni}/\text{Al}_2\text{O}_3$ and $16\text{Ni}_4\text{Fe}/\text{Al}_2\text{O}_3$ were 856.1 eV and 855.9 eV, respectively, which were higher than that pure NiO (854.4 eV) and NiAl_2O_4 (856.2 eV) [37], indicating that there might be two kinds of Ni species (NiO and NiAl_2O_4) on the surface of catalysts. The large amount of NiO could be formed by reoxidation of metallic Ni through contacting oxygen in air during the XPS experiments [38]. It could be noted that the binding energy of the $\text{Ni } 2p_{3/2}$ peak of $16\text{Ni}/\text{Al}_2\text{O}_3$ sample was slightly higher than that of $16\text{Ni}_4\text{Fe}/\text{Al}_2\text{O}_3$, which could be attributed to the stronger interaction between Ni and support in $16\text{Ni}/\text{Al}_2\text{O}_3$ [39].

TABLE 3: Gaussian fitting analysis of H₂-TPR patterns of 16Ni_xFe/Al₂O₃ catalysts.

Catalyst	H ₂ -consumption (mmol/g)			Reduction temperature (°C)/relative content (%)				
	Total	Reduced Fe ^a	Reduced Ni	α	β	γ	Peak I	Peak II
16Ni/Al ₂ O ₃	2.04	—	2.04	432.4/33.0	500.5/35.8	570.9/31.2	—	—
16Ni1Fe/Al ₂ O ₃	2.13	0.06	2.07	396.9/34.4	485.3/39.6	573.4/23.0	321.1/2.3	520.1/0.7
16Ni2Fe/Al ₂ O ₃	2.36	0.25	2.11	381.3/36.5	486.8/41.7	609.0/12.5	281.3/6.2	496.0/3.1
16Ni4Fe/Al ₂ O ₃	2.52	0.36	2.16	355.3/37.4	481.5/45.3	601.0/7.4	339.2/6.3	483.5/3.5
16Ni6Fe/Al ₂ O ₃	2.59	0.47	2.12	347.4/38.6	460.6/38.7	591.4/6.7	312.0/10.9	454.2/5.2
16Ni8Fe/Al ₂ O ₃	2.80	0.56	2.24	351.6/40.2	455.5/35.3	617.5/4.2	310.2/11.9	492.7/8.4
8Fe/Al ₂ O ₃	0.56	0.56	—	—	—	—	349.9/66.3	521.8/33.7

^aThe value calculated by different Fe content based on the H₂-consumption of 8Fe/Al₂O₃ catalyst.

As expected, catalyst 16Ni4Fe/Al₂O₃ possessed slightly higher Ni/Al atomic ratio (0.085) than that of 16Ni/Al₂O₃ (0.082), indicating that the introduction of Fe improved the dispersion of Ni species on the surface of catalyst 16Ni4Fe/Al₂O₃, which was in accordance with the results of XRD, H₂-TPR, and BET.

4. Conclusions

The catalytic performance of catalyst 16Ni_xFe/Al₂O₃ for CO methanation in slurry-bed reactor was greatly influenced by the content of iron. The introduction of iron improved the dispersion of Ni species and decreased the reduction temperature, and Ni-Fe alloy was formed when the content of iron exceeded 2%, which was favorable for the methanation of CO. With the increase of iron content, the catalytic performance of CO methanation increased at first and then decreased. Excessive iron content covered the active component Ni and aggravated the water gas shift reaction.

Conflict of Interests

The authors declare that they have no conflict of interests regarding the publication of this paper.


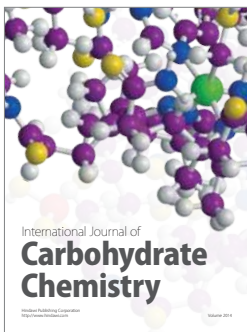
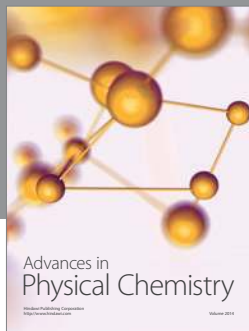
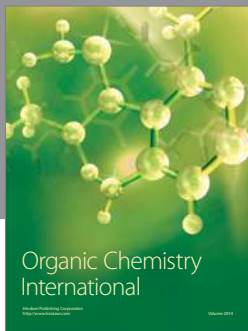
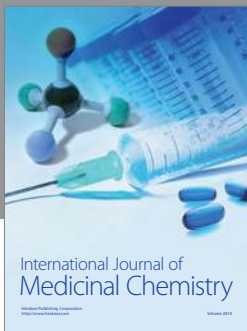
Acknowledgments

This work was supported by the National Basic Research Program of China (973 Program, no. 2012CB723105), Youth Foundation of Shanxi Province (no. 2013021007-4), China Postdoctoral Science Foundation (no. 2013M541210), and Youth Foundation of Taiyuan University of Technology (no. 2012L040). The authors gratefully appreciate the help from Li Congming (Japan Gas Synthesis CO. LTD) for the grammar and technical check.

References

- [1] J. Kopycinski, T. J. Schildhauer, and S. M. A. Biollaz, "Production of synthetic natural gas (SNG) from coal and dry biomass—a technology review from 1950 to 2009," *Fuel*, vol. 89, no. 8, pp. 1763–1783, 2010.
- [2] J. Zhang, N. Fatah, S. Capela, Y. Kara, O. Guerrini, and A. Y. Khodakov, "Kinetic investigation of carbon monoxide hydrogenation under realistic conditions of methanation of biomass derived syngas," *Fuel*, vol. 111, pp. 845–854, 2013.
- [3] G. Q. Zhang, T. J. Sun, J. X. Peng, S. Wang, and S. D. Wang, "A comparison of Ni/SiC and Ni/Al₂O₃ catalyzed total methanation for production of synthetic natural gas," *Applied Catalysis A: General*, vol. 462–463, pp. 75–81, 2013.
- [4] A. M. Zhao, W. Y. Ying, H. T. Zhang, H. F. Ma, and D. Y. Fang, "Ni/Al₂O₃ catalysts for syngas methanation: effect of Mn promoter," *Journal of Natural Gas Chemistry*, vol. 21, no. 2, pp. 170–177, 2012.
- [5] M. C. Seemann, T. J. Schildhauer, and S. M. A. Biollaz, "Fluidized bed methanation of wood-derived producer gas for the production of synthetic natural gas," *Industrial and Engineering Chemistry Research*, vol. 49, no. 15, pp. 7034–7038, 2010.
- [6] J. Li, L. Zhou, P. C. Li et al., "Enhanced fluidized bed methanation over a Ni/Al₂O₃ catalyst for production of synthetic natural gas," *Chemical Engineering Journal*, vol. 219, pp. 183–189, 2013.
- [7] B. Liu and S. F. Ji, "Comparative study of fluidized-bed and fixed-bed reactor for syngas methanation over Ni-W/TiO₂-SiO₂ catalyst," *Journal of Energy Chemistry*, vol. 22, no. 5, pp. 740–746, 2013.
- [8] S. B. Alpert, M. B. Sherwin, and N. P. Cochran, "Slurry phase methanation process," US Patent 3989734, 1976.
- [9] Z. He, X. X. Cui, H. Fan, Y. Chang, and Z. Li, "Research of coal-to-synthetic natural gas technology and catalyst," *Chemical Industry and Engineering Progress*, vol. 30, no. S1, pp. 388–392, 2011.
- [10] Q. G. Zhang, Z. Li, S. W. Yan et al., "Process for synthesizing natural gas by methanation of coal synthesis gas," CN Patent 101979476, 2011.
- [11] L. He, Y. G. Wang, W. B. Gong, F. F. Yang, D. P. Xu, and H. Y. Zhang, "Research of the catalysts for methanation in slurry bed reactor," *Chemical Industry and Engineering Progress*, vol. 31, no. S1, pp. 311–314, 2012.
- [12] J. F. Zhang, Y. X. Bai, Q. D. Zhang, H. J. Xie, Y. S. Tan, and Y. Z. Han, "Low temperature methanation of syngas in a slurry reactor over Zr-doped Ni/ γ -Al₂O₃ catalyst," *Journal of Fuel Chemistry and Technology*, vol. 41, no. 8, pp. 966–971, 2013.
- [13] T. Bligaard, J. K. Nørskov, S. Dahl, J. Matthiesen, C. H. Christensen, and J. Sehested, "The Brønsted-Evans-Polanyi relation and the volcano curve in heterogeneous catalysis," *Journal of Catalysis*, vol. 224, no. 1, pp. 206–217, 2004.
- [14] S. Hwang, J. Lee, U. G. Hong et al., "Methane production from carbon monoxide and hydrogen over nickel-alumina xerogel catalyst: effect of nickel content," *Journal of Industrial and Engineering Chemistry*, vol. 17, no. 1, pp. 154–157, 2011.

- [15] D. C. Hu, J. J. Gao, Y. Ping et al., "Enhanced investigation of CO methanation over Ni/Al₂O₃ catalysts for synthetic natural gas production," *Industrial and Engineering Chemistry Research*, vol. 51, no. 13, pp. 4875–4886, 2012.
- [16] X. L. Yan, Y. Liu, B. R. Zhao, Z. Wang, Y. Wang, and C. J. Liu, "Methanation over Ni/SiO₂: effect of the catalyst preparation methodologies," *International Journal of Hydrogen Energy*, vol. 38, no. 5, pp. 2283–2291, 2013.
- [17] A. L. Kustov, A. M. Frey, K. E. Larsen, T. Johannessen, J. K. Nørskov, and C. H. Christensen, "CO methanation over supported bimetallic Ni-Fe catalysts: from computational studies towards catalyst optimization," *Applied Catalysis A: General*, vol. 320, pp. 98–104, 2007.
- [18] S. Hwang, U. G. Hong, J. Lee et al., "Methanation of carbon dioxide over mesoporous Nickel-M-Alumina (M=Fe, Zr, Ni, Y, and Mg) xerogel catalysts: effect of second metal," *Catalysis Letters*, vol. 142, no. 7, pp. 860–868, 2012.
- [19] S. Hwang, J. Lee, U. G. Hong et al., "Hydrogenation of carbon monoxide to methane over mesoporous nickel-M-alumina (M=Fe, Ni, Co, Ce, and La) xerogel catalysts," *Journal of Industrial and Engineering Chemistry*, vol. 18, no. 1, pp. 243–248, 2012.
- [20] D. Y. Tian, Z. H. Liu, D. D. Li, H. L. Shi, W. X. Pan, and Y. Cheng, "Bimetallic Ni-Fe total-methanation catalyst for the production of substitute natural gas under high pressure," *Fuel*, vol. 104, pp. 224–229, 2013.
- [21] P. Z. Zhong, F. H. Meng, X. X. Cui, J. Liu, and Z. Li, "Catalytic performance of Ni-Fe/ γ -Al₂O₃ catalyst prepared from different nickel precursors for CO methanation," *Chemical Industry and Engineering Progress*, vol. 32, no. 8, pp. 1845–1848, 2013.
- [22] J. Liu, F. H. Meng, P. Z. Zhong, K. M. Ji, and Z. Li, "Effect of support texture properties on Ni-Fe/ γ -Al₂O₃ catalyst structure and catalytic performance for CO methanation," *Natural Gas Chemical Industry*, vol. 38, no. 4, pp. 6–10, 2013.
- [23] C. Rhodes, G. J. Hutchings, and A. M. Ward, "Water-gas shift reaction: finding the mechanistic boundary," *Catalysis Today*, vol. 23, no. 1, pp. 43–58, 1995.
- [24] K. Y. Koo, H.-S. Roh, U. H. Jung, and W. L. Yoon, "Combined H₂O and CO₂ reforming of CH₄ over Ce-promoted Ni/Al₂O₃ catalyst for gas to liquid (GTL) process: enhancement of Ni-CeO₂ interaction," *Catalysis Today*, vol. 185, no. 1, pp. 126–130, 2012.
- [25] A. Iriondo, V. L. Barrio, J. F. Cambra et al., "Hydrogen production from glycerol over nickel catalysts supported on Al₂O₃ modified by Mg, Zr, Ce or La," *Topics in Catalysis*, vol. 49, no. 1–2, pp. 46–58, 2008.
- [26] H. Wang, Y. Z. Fang, Y. Liu, and X. Bai, "Perovskite LaFeO₃ supported bi-metal catalyst for syngas methanation," *Journal of Natural Gas Chemistry*, vol. 21, no. 6, pp. 745–752, 2012.
- [27] F. Y. Sun, M. Wu, W. Z. Li, X. Y. Li, W. Z. Gu, and F. D. Wang, "Relationship between crystallite size and photocatalytic activity of titanium dioxide," *Chinese Journal of Catalysis*, vol. 19, no. 3, pp. 229–233, 1998.
- [28] B. Tang, Q. Jiang, X. W. He, and H. X. Shen, "Study on the surface diffuse reflectance ultraviolet-visible spectra of the multicomponent metal catalysts," *Spectroscopy and Spectral Analysis*, vol. 19, no. 1, pp. 100–101, 1999.
- [29] N. Malengreau, J.-P. Muller, and G. Calas, "Fe-speciation in kaolins: a diffuse reflectance study," *Clays & Clay Minerals*, vol. 42, no. 2, pp. 137–147, 1994.
- [30] X. Hu, L. J. Zhang, and G. X. Lu, "Pruning of the surface species on Ni/Al₂O₃ catalyst to selective production of hydrogen via acetone and acetic acid steam reforming," *Applied Catalysis A: General*, vol. 427–428, pp. 49–57, 2012.
- [31] R. Da Paz Fiuza, M. Aurélio Da Silva, and J. S. Boaventura, "Development of Fe-Ni/YSZ-GDC electrocatalysts for application as SOFC anodes: XRD and TPR characterization and evaluation in the ethanol steam reforming reaction," *International Journal of Hydrogen Energy*, vol. 35, no. 20, pp. 11216–11228, 2010.
- [32] S.-H. Kang, J.-H. Ryu, J.-H. Kim et al., "Co-methanation of CO and CO₂ on the Ni_x-Fe_{1-x}/Al₂O₃ catalysts; effect of Fe contents," *Korean Journal of Chemical Engineering*, vol. 28, no. 12, pp. 2282–2286, 2011.
- [33] W.-J. Wang and Y.-W. Chen, "Influence of metal loading on the reducibility and hydrogenation activity of cobalt/alumina catalysts," *Applied Catalysis*, vol. 77, no. 2, pp. 223–233, 1991.
- [34] J. Sehested, K. E. Larsen, A. L. Kustov et al., "Discovery of technical methanation catalysts based on computational screening," *Topics in Catalysis*, vol. 45, no. 1–4, pp. 9–13, 2007.
- [35] N. Wang, Z. J. Sun, Y. Z. Wang, X. Q. Gao, and Y. X. Zhao, "Preparation of bimetallic Ni-Fe/ γ -Al₂O₃ catalyst and its activity for CO methanation," *Journal of Fuel Chemistry and Technology*, vol. 39, no. 3, pp. 219–223, 2011.
- [36] Q. H. Liu, L. W. Liao, Z. L. Liu, and X. F. Dong, "Effect of ZrO₂ crystalline phase on the performance of Ni-B/ZrO₂ catalyst for the CO selective methanation," *Chinese Journal of Chemical Engineering*, vol. 19, no. 3, pp. 434–438, 2011.
- [37] S. B. Wang and G. Q. Lu, "Reforming of methane with carbon dioxide over Ni/Al₂O₃ catalysts: effect of nickel precursor," *Applied Catalysis A: General*, vol. 169, no. 2, pp. 271–280, 1998.
- [38] C. Guimon, A. Auroux, E. Romero, and A. Monzon, "Acetylene hydrogenation over Ni-Si-Al mixed oxides prepared by sol-gel technique," *Applied Catalysis A: General*, vol. 251, no. 1, pp. 199–214, 2003.
- [39] M. D. Cai, J. Wen, W. Chu, X. Q. Cheng, and Z. J. Li, "Methanation of carbon dioxide on Ni/ZrO₂-Al₂O₃ catalysts: effects of ZrO₂ promoter and preparation method of novel ZrO₂-Al₂O₃ carrier," *Journal of Natural Gas Chemistry*, vol. 20, no. 3, pp. 318–324, 2011.



Hindawi

Submit your manuscripts at
<http://www.hindawi.com>

